POLITECNICO DI TORINO
Repository ISTITUZIONALE

Impact of bidirectional EV charging stations on a distribution network: a Power Hardware-In-the-Loop implementation

Original
Impact of bidirectional EV charging stations on a distribution network: a Power Hardware-In-the-Loop implementation / Benedetto, G., Bompard, E., Mazza, A., Pons, E., Jaboeuf, R., Tosco, P., Zampolli, M.. - In: SUSTAINABLE ENERGY, GRIDS AND NETWORKS. - ISSN 2352-4677. - ELETTRONICO. - 35:(2023), pp. 1-12. [10.1016/j.segan.2023.101106]

Availability:
This version is available at: 11583/2980567 since: 2023-07-26T07:02:19Z

Publisher:
Elsevier

Published
DOI:10.1016/j.segan.2023.101106

Terms of use:

This article is made available under terms and conditions as specified in the corresponding bibliographic description in the repository

Publisher copyright

(Article begins on next page)

08 November 2026

Sustainable Energy, Grids and Networks 35 (2023) 101106

Contents lists available at ScienceDirect

Sustainable Energy, Grids and Networks

journal homepage: www.elsevier.com/locate/segan

Impact of bidirectional EV charging stations on a distribution network: a Power Hardware-In-the-Loop implementation

Giorgio Benedetto [a], Ettore Bompard [a], Andrea Mazza [a,*], Enrico Pons [a], Rémi Jaboeuf [b], Paolo Tosco [b], Marco Zampolli [b]

[a] Dipartimento Energia and Energy Center Lab, Politecnico di Torino, C.so Duca degli Abruzzi, 24, Torino, 10129, Italy
[b] Research, Development and Techn. Innovation Dep., Edison SpA, Foro Buonaparte 31, Milano, 20121, Italy

ARTICLE INFO

Article history:
Received 8 February 2023
Received in revised form 5 May 2023
Accepted 18 June 2023
Available online 5 July 2023

Keywords:
Vehicle-to-grid
Grid-to-vehicle
Real-time simulation
Power hardware-in-the-loop
Low-voltage system
Battery electric vehicles
Power quality
Harmonics

ABSTRACT

The need for decarbonizing the entire energy system calls for new operational approaches in different sectors, currently (almost) fully dominated by fossil fuels, such as the transports. In particular, the decarbonization of the light-duty passenger transport, based on the implementation of Battery Electric Vehicles, may have a twofold benefit, because of (i) the reduction of local and global direct emissions, and (ii) the role that the Battery Electric Vehicles can have in supporting the operation of the power system in case of large share of non-dispatchable renewable energy sources. This paper aims to investigate, through a Power Hardware-In-the-Loop laboratory setup, the impacts of the Vehicle-to-Grid and Grid-to-Vehicle paradigms on a Low Voltage grid portion serving as grid infrastructure a car parking. The results show that the Low Voltage grid losses, if not taken into account, can cause a wrong evaluation of the expected impact on the grid of the Battery Electric Vehicles. Furthermore, the harmonics of current injected into the grid by several chargers could compromise the perceived power quality. Both the analyzed aspects must be hence carefully considered for properly evaluating pros and cons that the installation of several chargers may have on the grid side. The main contributions refer to the calculation of losses and to the evaluation of the power quality aspects through a Power Hardware-In-the-Loop configuration, enabling to take into account the interaction between charging stations and power grid.

© 2023 The Author(s). Published by Elsevier Ltd. This is an open access article under the CC BY-NC-ND license (http://creativecommons.org/licenses/by-nc-nd/4.0/).

1. Introduction

The decarbonization process and the electrification of consumption are bringing new challenges to the electricity network. On the one hand, Renewable Energy Sources (RES) are penetrating more and more in the energy generation mix, so new strategies have to be developed, thanks also to the active involvement of consumers (prosumers), trying to improve the quality of the electricity service even in cases of emergency [1].

On the other hand, since 2019 the sale of Electric Vehicles (EVs) has grown and the total sales are expected to increase at steeper rate to 11.2 million in 2025 and 31.1 million by 2030 [2]. This could lead the total load to increase. In the studies [3] and [4] some projections of the increasing electricity demand are reported: the major concern is the effect it will have on the load profile of the network and the consequent impacts on the Medium Voltage (MV) and Low Voltage (LV) distribution systems [5,6]. More power withdrawn may also cause the overload of the distribution transformers: this can increase the accelerated ageing of the transformers, and hence their loading level must be carefully evaluated.

The primary objective of an Electric Vehicle Charging Station (EVCS) is to charge the EV battery. However, a bidirectional charging station can provide some others additional services, grouped under the acronym Vehicle-to-X (V2X) [7]. In fact, the vehicles can interact with the charging infrastructure at various levels: an example is the Vehicle-to-Home (V2H) paradigm, where the car can provide energy to the house. Another example refers to the well-known V2G, where the cars can inject energy into the distribution grid, contributing to the provision of the grid ancillary services. Some examples of services that the V2G may provide are: (i) *Frequency Regulation Service*, requiring high power for relatively short time, usually 10–15 min [8]; (ii) *Voltage support*, with V2G injecting or absorbing reactive power in order to control the grid voltage, and (iii) *Peak shaving/valley filling*, where EVs can modify its consumption/injection, by modifying the load profile.

Exploiting and catching all the above new opportunities requires the development of new management strategies and the installation of new devices, able to make the power grids ready to handle with new business opportunities that are now possible.

* Corresponding author.
E-mail address: andrea.mazza@polito.it (A. Mazza).

https://doi.org/10.1016/j.segan.2023.101106
2352-4677/© 2023 The Author(s). Published by Elsevier Ltd. This is an open access article under the CC BY-NC-ND license (http://creativecommons.org/licenses/by-nc-nd/4.0/).

Nomenclature

ΔV	Voltage drop.
P_{ist}	Total load active power.
S	Total load apparent power.
V_{sim}	Single phases voltages the ending node.
v_j	Voltage of phase j.
i_j	Current of phase j.
I	Total load current.
T_s	Simulation time step.

Acronyms

BESS	Battery Energy Storage System
BFS	Backward Forward Sweep
CHIL	Controller Hardware-In-The-Loop
DSO	Distribution System Operator
DUT	Device Under Test
EV	Electric Vehicle
EVCS	Electric Vehicle Charging Station
FFT	Fast Fourier Transformation
G2V	Grid-to-Vehicle
HIL	Hardware-In-the-Loop
HV	High Voltage
ITM	Ideal Transformer Model
LV	Low Voltage
MV	Medium Voltage
PCC	Point of Common Coupling
PEM	Proton-Exchange Membrane
PHIL	Power Hardware-In-the-Loop
RES	Renewable Energy Sources
RTS	Real-time Simulation
SOC	State Of Charge
THD	Total Harmonic Distortion
V2X	Vehicle-to-X
V2H	Vehicle-to-Home
V2B	Vehicle-to-Building
V2G	Vehicle-to-Grid
WB	WallBox

However, the upgrade of a complex infrastructure as power systems needs huge investments, which must be justified only after the evaluation of the benefits that any innovation may generate. Hence, the deployment of new systems requires reliable and repeatable tests and validations procedure before being actually implemented. This involves a mandatory testing process of the selected hardware in the environment within it has to be installed. For EVCS, the main issue is the evaluation of the impact of more units on the distribution grid, in terms of voltage level, losses, and disturbances injected into the grid. Different methods can be used to evaluate the above cited aspects. A possible approach is to measure the electrical quantities directly on the device, like in [9], which presents a unified method for measuring the efficiency of chargers for mass-produced EVs. The method is validated through extensive tests of the Renault Zoe, Nissan LEAF, and Peugeot iOn models. The results show a non-negligible loss, resulting in unnecessary energy consumption, and increased load on the grid. Other works, as [10], assess the disturbances on LV Residential Network, investigating the expected increase of EV penetration. The authors present the estimation of current harmonic injection of EVs charging with different voltage distortions and examine the impact of EVs charging on the distribution transformer with a load flow approach. Also in [11] the impact on the LV grid is studied. The paper highlights the possible developments in primary and secondary supra-harmonic emissions either in a conventional or power-electronic-dominated system and the interactions between devices, which may result in tripping of residual current devices. The results of the measurements suggest that the supra-harmonic currents mainly remain within the local installation, and that the level of voltage distortion depends on the connection impedance. Consequently, in order to achieve power network simulations as close as possible to the real world and to interconnect a real hardware device to the simulation, Real-time Simulation (RTS) and Power Hardware-In-the-Loop (PHIL) can be used, being the most effective and reliable way to achieve all these requirements. In [12] a comprehensive study of a PHIL testbed used for evaluating grid-connected EVCS is assessed. The PHIL testbed consists of two components: a PHIL-based battery emulator and a grid emulator, which simulate the behavior of a BESS and a LV grid, respectively. The authors develop a mathematical model to analyze the stability and accuracy of the PHIL testbed. The PHIL platform is validated using a RTS, and the validated test is employed to analyze the performance of a commercial EV charger and its interactions with a weak LV network. In [13] a Controller Hardware-In-The-Loop (CHIL) architecture is used for evaluating the impact of high-power vehicle charging stations on the grid. The CHIL platform captures real-time interactions between the grid, vehicle, and charger controller to evaluate the impact of charging load on the grid in terms of voltage variations and line congestion. The authors present experimental results to demonstrate the effectiveness of the proposed method in a laboratory environment. This paper presents the results of the study carried out at the Global Real-Time Superlab (G-RTSLAB) [14] at the Energy Center of Politecnico di Torino in collaboration with the company Edison SpA. The study aims at evaluating the impact of a EVCS group on a sample of LV distribution network in terms of voltage profile, power losses, power factor of the WallBox (WB) aggregation and injection of current harmonics . RTS with PHIL has been chosen as the methodology, instead of performing a steady state study as in [15], for two main reasons:

- *Temporal granularity of losses*: the value of the losses is updated at each simulation step and it is therefore possible to evaluate the management of the plant in real-time (i.e., in terms of power instead of energy).
- *Distortion introduced by a specific hardware*: the integration of power electronics in the grid, such as those found in WBs, causes harmonic distortion of the injected current and, consequently, of the voltage at the various nodes of the network. On the one hand, the presence of these harmonics increases both the losses and voltage drop with respect to the ideal case. These aspects are difficult to estimate through the analysis of the system by means of the steady-state solution through the Backward Forward Sweep (BFS) algorithm. Conversely, the PHIL configuration enables to connect the real device (i.e., the WB) and hence inject distorted currents into the simulated network. This leads to an easy estimation of the harmonic impact on the electrical quantities by measuring voltage and current in the simulation. Moreover, as the WB is inserted *in-the-loop*, the harmonic distortion of the currents causes harmonic distortion on the voltages at the WB input, which impacts the WB's behavior itself.

In order to evaluate the effect on the network of a specific hardware the PHIL approach seems therefore the most suitable. In fact, unlike a steady state approach, coupling the real converter with the simulated network in a PHIL configuration, enables the evaluation of the disturbances introduced by the charger in a

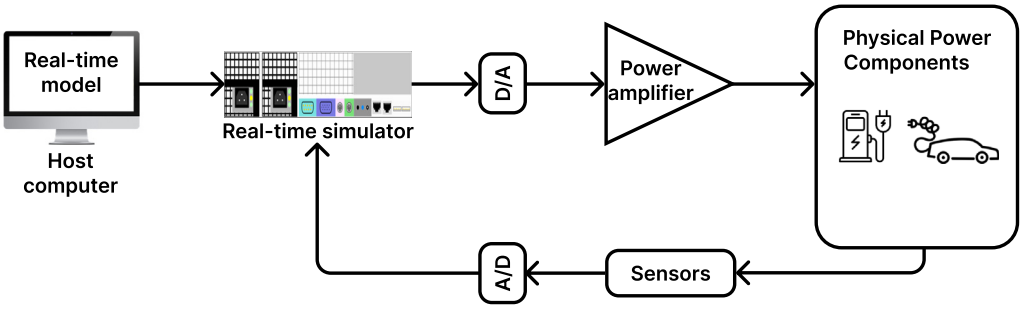

Fig. 1. PHIL simulation concept.

realistic environment. As in [16], the objective is to test the EVCS using the PHIL methodology under conditions which are as close as possible to the real application. In this work, two approaches are used: (i) the evaluation of the performance of the hardware directly measuring the electrical quantities on the real device and (ii) the study of the interaction of the converter with the power grid in a simulated environment. The EVCS will be supplied from a linear amplifier, enabling to control the input voltages and currents rather than test just the controller of the converter. Hence, unlike other works, the whole system composed of power grid, EVCS and EV will be analyzed.

The rest of the paper is organized as follows: Section 2 presents the concepts of RTS and PHIL and describes the laboratory layout used for the tests; Section 3 shows the distribution grid and the LV microgrid simulated in the RTS for the case study; in Section 4 the tests results are presented and discussed with reference to the voltage profiles, power losses, power factor and impact the of EVCSs on the network in terms of power quality; finally, the last section reports the conclusive remarks.

2. Overview of real-time simulation and power hardware-in-the-loop configuration usage for power system studies

2.1. Real-time simulation and power hardware-in-the-loop

Dynamic Simulations of electrical power systems enable solving real-world problems in a safe and repeatable way. There are two different types of dynamic simulations: offline simulations and online simulations [17]. In offline simulations the time required to solve all equations and functions describing the status of the entire system in a defined time step could exceed the duration of the time-step itself; hence both fixed and variable time-step resolution methods can be adopted. Conversely, in online simulations all the calculations are accomplished within the considered time-step, which must be properly fixed; if the time required exceeds the fixed step, an overrun occurs. This latter type of simulation is better known as RTS: a RTS enables to reproduce the behavior of a physical system through the execution of its computer-based model at the same speed of the actual time, so that each advancement in the simulation time is synchronous to the advancement of the real time (1:1 ratio with the wall-clock).

The main advantage of RTS is the possibility of replacing physical systems with virtual systems (models), as well as the insertion of external hardware to be tested in the simulation, the so called Device Under Test (DUT): this opportunity can mainly be achieved through the Hardware-In-the-Loop (HIL) and PHIL configuration. This enables the users to perform "in-silico" realistic closed loop tests without the need to install the DUT in the real power grid [18]. HIL refers to setups with low voltage and low power signal connections with the DUT, whereas PHIL can be employed for higher power testing. PHIL requires the creation of a virtual power interface between the RTS and DUTs. Typically, the power interface involves linear or switching power amplifiers and voltage and/or current sensors [17], as shown in Fig. 1.

PHIL can be useful for testing the impact of new technologies on large-scale grids in Real-Time, in a laboratory environment, and in a reliable and repeatable way. The PHIL concept is already proven and adapted in a larger number of application and some examples are reported in literature. In [19] a PHIL test-bed is designed to model and test grid-connected battery energy storage systems in power system application. In [20] PHIL simulation is used to validate two commercial photovoltaic inverters. In [21] two of the most popular variable-speed wind turbines are studied: the doubly-fed induction generator with partial-scale power converter and the permanent-magnet synchronous machine with full-scale power converter. In [22] a RTS and a PHIL simulation method of a Proton-Exchange Membrane (PEM) fuel cell stack system for emulating its electrical dynamics has been presented. Regarding specifically the charging systems of electric vehicles, the authors in [23] present a comprehensive small signal model capable of describing the dynamics of a PHIL test-bed developed for evaluating grid-connected EV chargers and, to conclude, in [24] a PHIL demonstrator is developed for the purpose of studying the impact of EV charging on LV distribution grids.

2.2. Interfacing the DUT in PHIL simulation

The connection between the simulation and the DUT is established through interface algorithms. Interface algorithms provide the means of relating simulated voltage and currents at the point of coupling between the RTS and the DUT to the measured voltage and current of the PHIL amplifier. This element is critical for the stability and accuracy of the PHIL simulation [25]. There are some possible configurations as reported in [18,25,26]: the one used in this work is the Ideal Transformer Model (ITM) interface algorithm, which is the simplest and straightforward method to connect the hardware side to the simulation in PHIL applications. The power amplifier receives the reference voltage signals from the real-time simulator and provides power to the DUT [18]; in the meantime, the current sensors measure the current signals on the DUT and feed them back to the real-time simulator through ideal current generators. Fig. 2 shows the PHIL implementation scheme of the ITM algorithm, where the physical hardware components (power amplifier and DUT) are highlighted in blue.

The elements denoted as $\dot{Z}_s$ and $\dot{Z}_L$ represent the equivalent Thévenin network parameters and the load parameters, respectively. It is worth noting that we cannot here call them impedances because the circuit is represented in the time domain. By the way, in the frequency domain, they would be impedances.

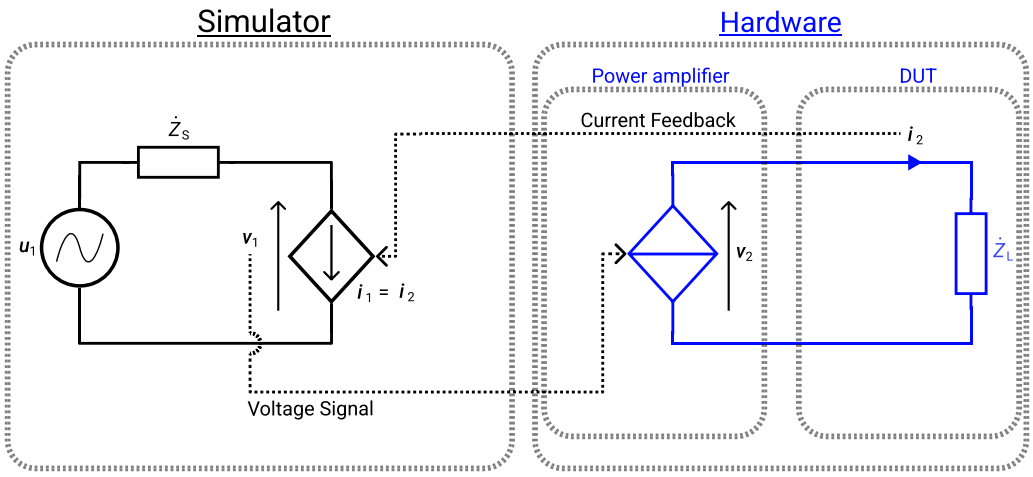

Fig. 2. PHIL Implementation scheme. (For interpretation of the references to color in this figure legend, the reader is referred to the web version of this article.)

2.3. Laboratory layout

The laboratory layout, as described in [27], exploits the real-time simulators capability to interface a real charging station to the simulated network. The role of the real-time simulator is essential to interface physical hardware components with a simulation environment, i.e., Simulink/Simscape in the performed tests. In order to guarantee a proper connection, the computation time step (T_s) should be carefully chosen: in fact, the smaller is the time step, the smaller is the introduced error, as the network solution is only calculated at discrete equidistantly spaced (and relatively close) simulation time points [28].

The main components used to carry out the tests are:

- *Real time simulator.* An OPAL-RT OP5700 has been used to load and run the model developed in the Simulink environment. The developed model is described in Section 3. The integration time step of the simulation was set to $T_s = 50\ \mu s$ in order to guarantee reliable results and a sufficient idle time to exlude the generation of computational overruns. Additional details on the RTS setup can be found in [27].
- *Power amplifier.* A linear power amplifier has been used. This technology has been chosen because of its high dynamic performance. The short time delay introduced enables the use of a simpler interface topology and guarantees less instability issues.
- *Charging station and electric vehicle.* The car used is a Nissan Leaf, which has a 62 kWh battery and uses the DC CHAdeMO plug. The model of charging station cannot be disclosed for confidentiality reasons. It is a bi-directional WB, with rated power 11 kW in G2V and 10 kW in V2G operation.

3. Modeled network layout

3.1. MV network layout

The chargers group is connected to a terminal node of one of the MV lines of the simulated distribution network. The MV side is based on real data provided by Turin Distribution System Operator (DSO). It is composed of five feeders, connected to the High Voltage (HV) grid through three HV/MV transformers. The WB group is then "installed" at the terminal node of the Brenta feeder. In Fig. 3 each node represents a MV/LV substation.

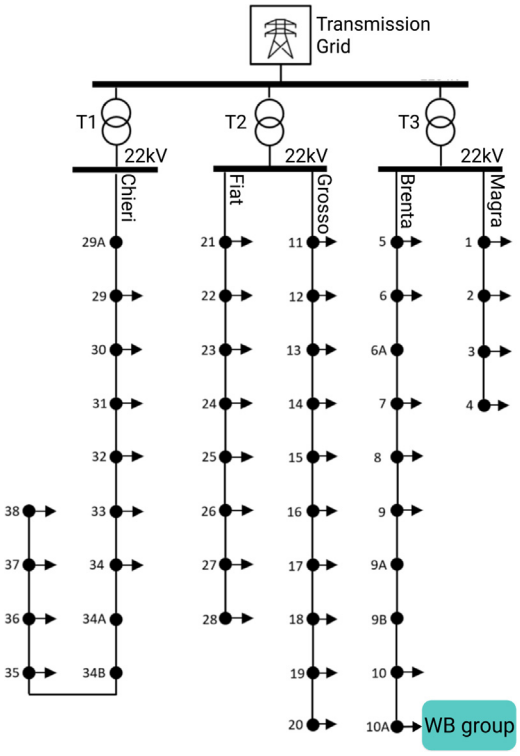

Fig. 3. MV distribution network layout.

3.2. Lv microgrid layout

The analyzed microgrid would emulate a plant constituted by several EVCSs, which have the capability to work in V2G mode in order to be a player at the ancillary services market. The first tested layout is constituted by five groups of four chargers each, which can be independently switched on or off to guarantee 200 kW of injected power. The tests have been conducted on a single real charger, so each group contributes to the total load multiplying the real measured currents, fed back into the simulation, by a gain of four. All of them are connected to the MV section with a three phase LV line and a single transformer. This configuration lowers the cost of the components. The dry type transformer has a nominal power equal to 315 kVA, while the line derived by the transformer has a cross section of 240 mm^2. This

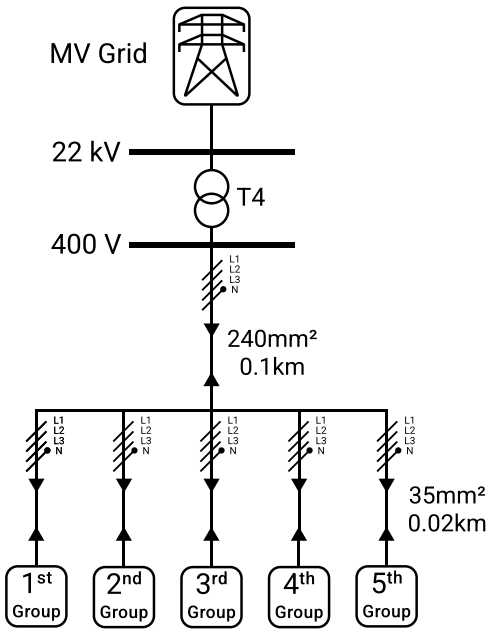

Fig. 4. LV microgrid layout.

line supplies a busbar, from which five lines of length 200 m and cross section 35 mm^2 are derived. Fig. 4 shows the layout of the LV section.

4. Results

The performed tests aim to highlight the magnitude of the impacts that a group of WBs has on both LV and MV networks in different load conditions, in order to evaluate if and how a similar infrastructure could be connected to the real distribution grid. The tests are focused on the Brenta MV line (which is connected to the tested load) and the Magra one (because supplied by the same HV/MV transformer). The electric quantities are measured in different points on the two MV distribution feeders simulated in the RTS, as shown in Fig. 5, and captured for a short time period in steady state conditions, i.e. three seconds, to represent a snapshot of the worst operation conditions. At the end of the Brenta feeder, the groups of WBs are represented through a box highlighted in blue, in order to distinguish the real tested hardware from the simulated system (in black).

4.1. Extrapolated EV charger control

From the experimental tests carried out on the real WB, it has been deduced that it is equipped with a resonant control, similar to the one belonging to a load emulator, shown in Fig. 6 [29], which, in our preliminary tests, has shown a behavior very similar to the DUT's one.

This kind of control algorithms is structured in block resonating at a given frequency. Within the resonant frequency, each block enables the suppression of gain and phase errors of the current, so each harmonic can be controlled independently.

4.2. Voltage and current values in presence of more EV chargers and harmonic content

In a real application the State Of Charge (SOC) of the cars, the chargers' power set-points and therefore the phases of the harmonics of different chargers are unpredictable. In the presented case study, the total load is obtained by multiplying the measured currents of the real hardware, so the amplitude and the phases of the disturbances generated by every charger are exactly the same, similar to the case shown in [30]. As said in [31], different phases can lead to harmonics sum or cancellation; however, by multiplying the same currents with the same amplitudes and phase angles, the summation of two harmonics with the same frequency is certain. Moreover, [30,32] show that ignoring the diversity among distributed harmonic sources (such as EV battery chargers), leads to a significant overestimation of the harmonic problem.

Furthermore, in [31] some electric vehicle chargers are tested and it has been observed that all phase angles of the different harmonic frequencies vary within a defined range: the phase angles actually tend to have a higher density around an average value strictly depending on the installed hardware. In this context it is reasonable to say that the existing harmonics will tend to sum one to each other up, especially assuming a high number of connected WBs.

Regarding the voltage value, in the simulated MV and LV distribution grid portions, the twenty chargers are installed under the same MV/LV transformer and are connected with LV cables to emulate the parking lot LV distribution system. For this reason, the voltage supply will be almost the same for all the units.

4.2.1. Harmonic interaction

According to has been presented in Section 4.2, the sum of the current harmonics is assumed for all the frequencies. Two different situations can be highlighted:

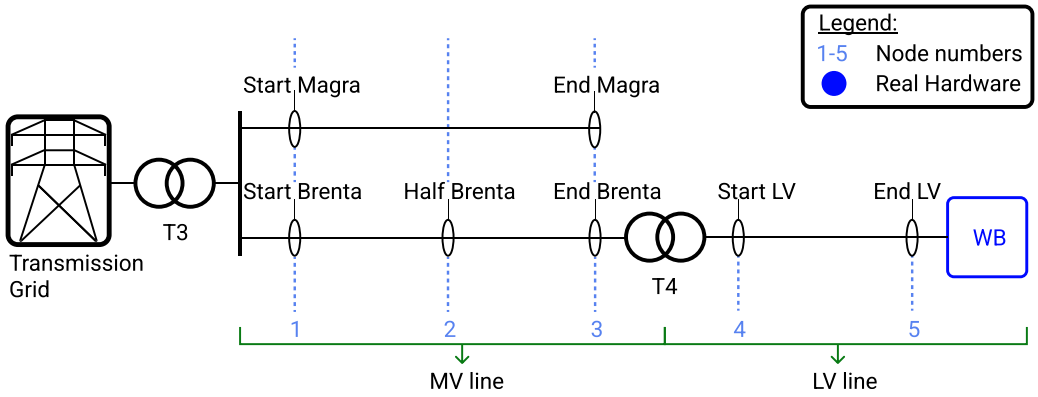

Fig. 5. Measurement points position. (For interpretation of the references to color in this figure legend, the reader is referred to the web version of this article.)

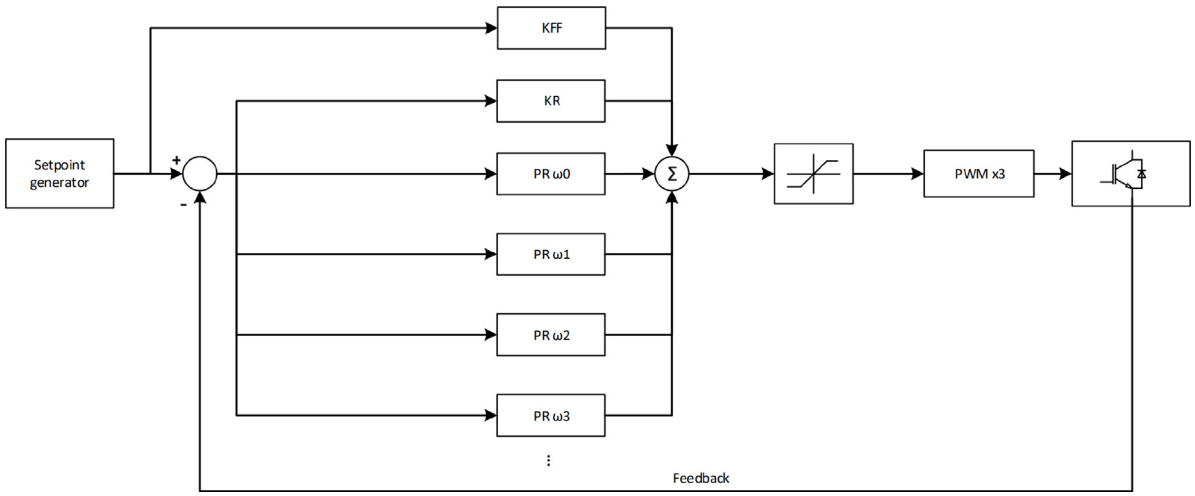

Fig. 6. Resonant control scheme example from [29].

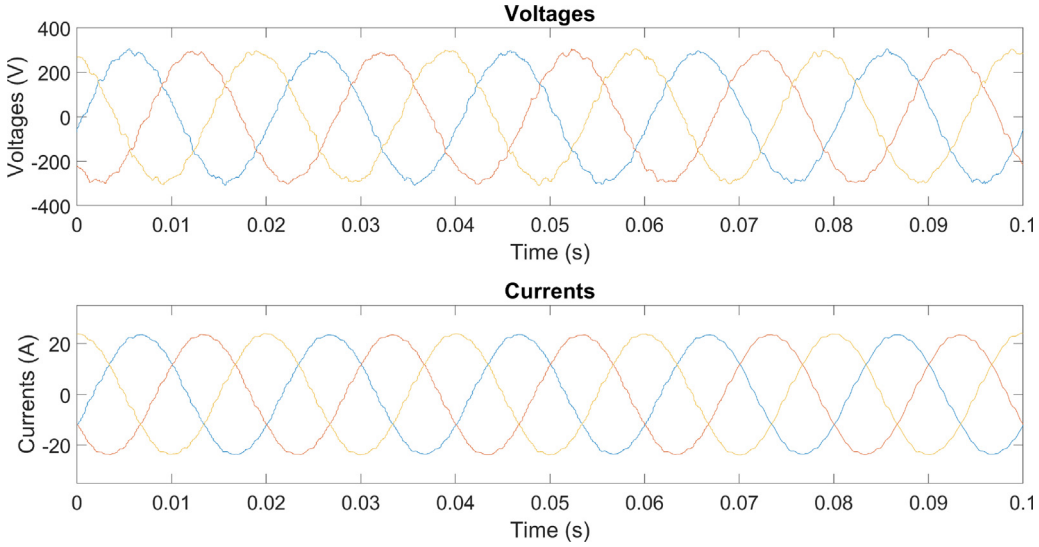

Fig. 7. *Case 1*: Voltages and currents of one charger in presence of twenty connected chargers.

- *Case 1*: the charger is fed with highly filtered voltages, so the impact of the injected disturbances is low. The filter cut off frequency is 500 Hz. This case did not show any stability issue, and all the twenty EV chargers can be connected.
- *Case 2*: the voltages are measured at the connection node of the simulated grid and, after a much weaker filtering (i.e., cut off frequency equal to 1 kHz), they are sent to the charger through the power amplifier. In this way, practically the entire disturbances are given to the charger, impacting its behavior. It is worth noting that, for stability reason, this case has been tested with only nineteen connected EV chargers.

Fig. 7, referring to *Case 1*, shows pretty much clear waveforms. In fact, the input voltages in this case were strongly filtered: this filtering decouples the converter and the grid, shifting the resonance frequency towards really high frequencies (well higher than 23th order).

The 23th harmonic order has a much higher impact in *Case 2*, as shown in Fig. 8. This behavior may depend by different factors, namely:

- the grid impedance and the modulating signal sampling frequency, as described in [33];
- the control strategy of the internal converter, which cannot control current harmonics higher than a specific order if the amplitude exceeds an extreme limit.

In particular, if the control fails with a specific harmonic order, that specific harmonic tends to diverge, even exceeding the value of the fundamental and hence becoming the fundamental component itself. This phenomenon is visible in Fig. 9, where the harmonic spectrum of the waveforms shown in Fig. 8 is depicted. The amplitude of the harmonics in Fig. 9 are the sum of the amplitudes of the harmonic with frequencies that cannot be properly controlled by the converter. The analyzed harmonic spectra had the same behavior on the three phases, so the following harmonic spectra refer to the current related to the phase #1.

The hereby presented interaction of the harmonics generated from the chargers are then considered as assumption for the following results. In the study, the harmonic interaction is considered on the current components: thus, in order to run stable simulation and to decouple the chargers from the grid, the filter on the input voltage has been kept with the cut off frequency equal to 500 Hz.

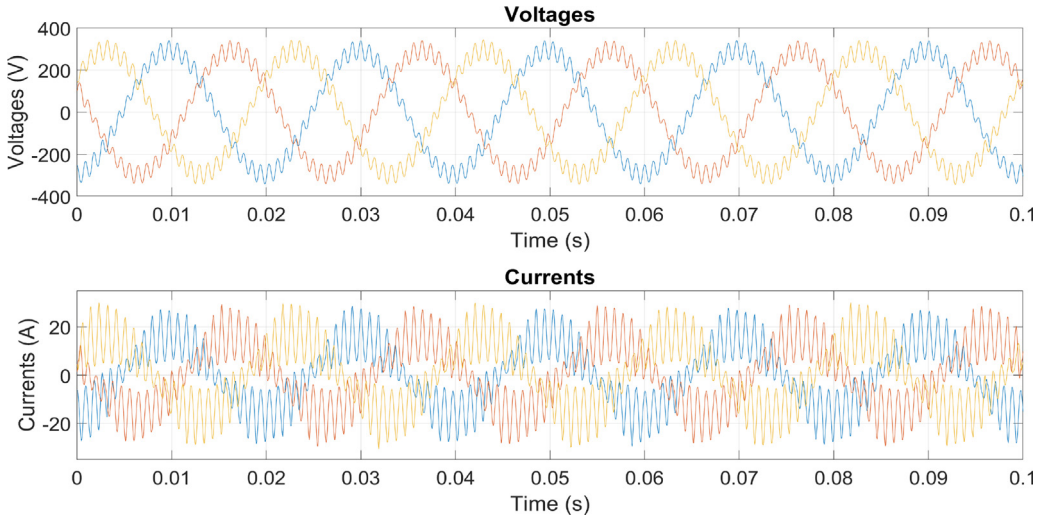

Fig. 8. *Case 2*: Voltages and currents of one charger in presence of nineteen connected chargers.

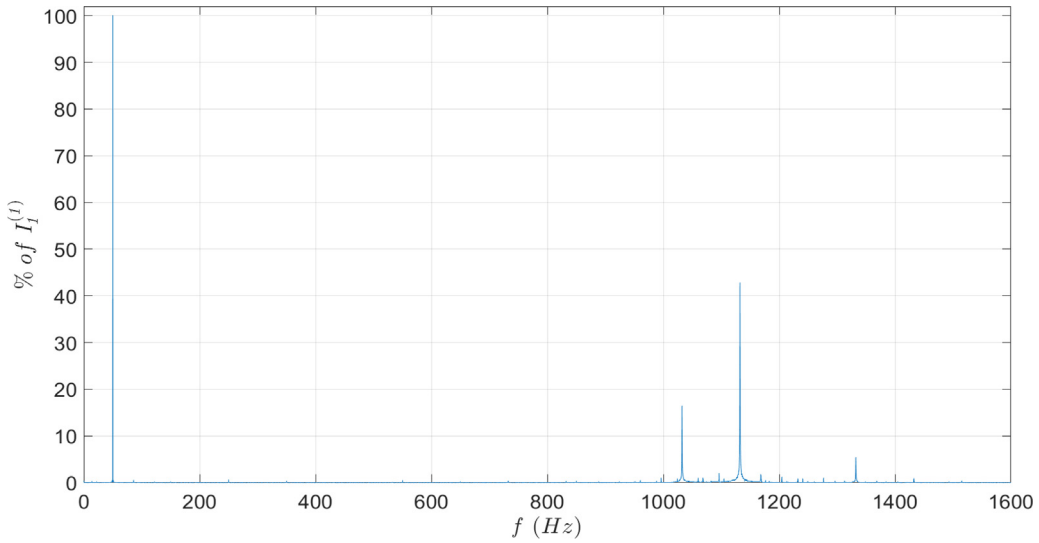

Fig. 9. *Case 2*: Current harmonic content at control limit. $I_1^{(1)}$ indicates the rms value of the fundamental component of the current related to the phase #1.

4.2.2. Total harmonic distortion indicators

In order to evaluate the impact of the EVCSs in terms of power quality, the Total Harmonic Distortion (THD) indicator is computed both for voltages and currents. It has been calculated on different points along the line to know if it remains under the value of 5% on the connection point. Even on the connection node of the closest MV feeder Magra has been verified: this last check is required for evaluating if and how much an adjacent line is affected in terms of power quality degradation due to the injected disturbances. The values of the average THD indicator, computed on the three phases, are shown in Table 1; in the table, the stand-by case is neglected because the THD must be evaluated only at the rated power.

As shown in Table 1, the value of 5% has never been exceeded both in G2V and V2G operations and, as expected, the highest values are measured on the points closest to the converters.

Table 1
Average THD for voltages and currents.

Component/Point of the system	Voltages THD %		Currents THD %	
	G2V	*V2G*	*G2V*	*V2G*
4 WB group	2.27	1.98	1.98	2.03
20 WB group	2.30	1.97	1.98	2.03
Start LV line	1.67	1.52	1.98	2.03
End MV line Brenta	0.22	0.22	1.96	2.06
Half MV line Brenta	0.22	0.22	0.25	0.25
Start MV line Brenta	0.21	0.22	0.20	0.21
Start MV line Magra	0.22	0.21	0.28	0.26
End MV line Magra	0.22	0.22	0.20	0.20

4.2.3. Compliance with the harmonic limits

The THD indicators are not sufficient to evaluate the quality of the waveforms, because, as stated in [34] for the connection of converters groups to the grid, the harmonics must be lower than specific levels with respect to the fundamental, as reported in Table 2. The suggested general procedure is presented in IEEE Std. 1547.1 Section 5.11 [35]: so, to perform the test, voltages and currents were obtained at the nominal power for both V2G and G2V. Then, a Fast Fourier Transformation (FFT) has been applied to retrieve the harmonic components.

The harmonic spectrum for the currents of the twenty WBs, which results the worst case in terms of measured disturbances,

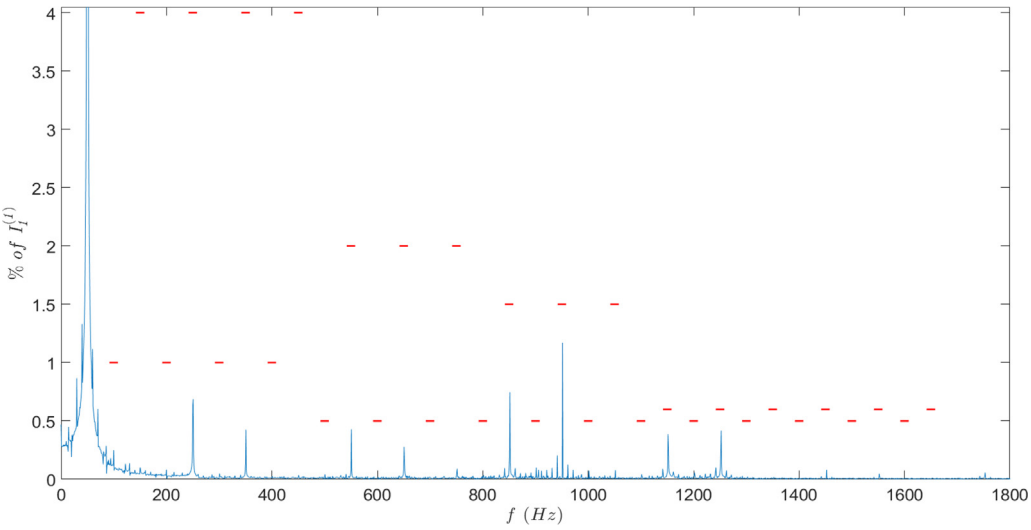

Fig. 10. Twenty WBs harmonic profile with limits while operating in G2V mode. $I_1^{(1)}$ indicates the rms value of the fundamental component of the current related to the phase #1. (For interpretation of the references to color in this figure legend, the reader is referred to the web version of this article.)

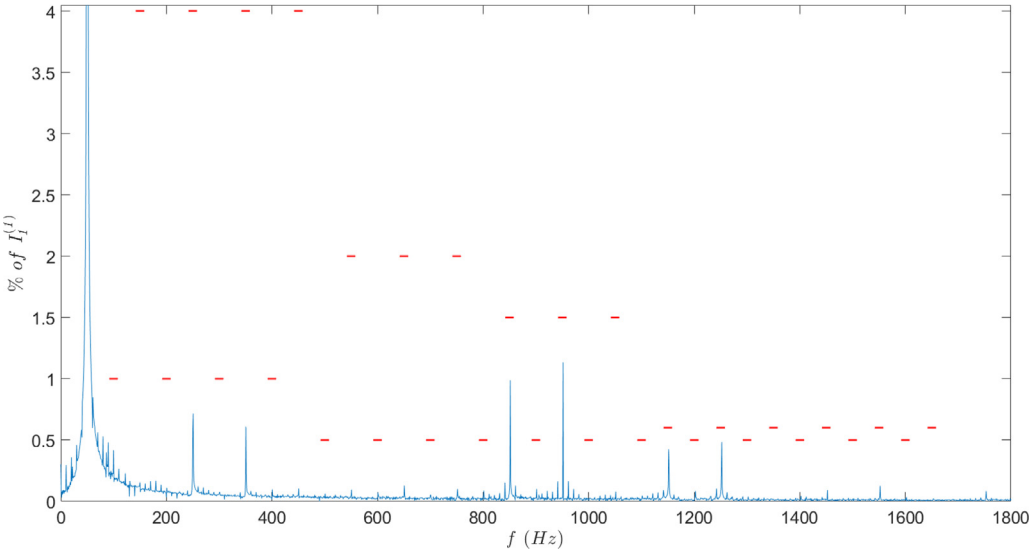

Fig. 11. Twenty WBs harmonic profile with limits while operating in V2G mode. $I_1^{(1)}$ indicates the rms value of the fundamental component of the current related to the phase #1. (For interpretation of the references to color in this figure legend, the reader is referred to the web version of this article.)

Table 2
Harmonics amplitude limits, provided as % of the fundamental.

Odd harmonics	Distortion limits %
3th to 9th	4%
11th to 15th	2%
17th to 21th	1.5%
23th to 33th	0.6%
Even harmonics	
2th to 8th	1%
10th to 32th	0.5%

is shown in Figs. 10 and 11 for G2V and V2G operation, respectively. In the two figures, the prescribed limits for each harmonic order are highlighted by red bars.

4.2.4. Stand-by operation

The harmonic spectrum for the WBs in stand-by operation is reported in Fig. 12. In this case, the THD indicator is not totally reliable because, in low load conditions, the ratio between the harmonics and fundamental is higher than in full load applications (due to the low amplitude of the latter one). However, in the simulated scenario, the total stand-by load could be a non-negligible operating condition, in particular if we assume a high number of EVCSs typical of a real application.

4.3. Voltage profile

The connection of twenty simulated EVs might have an adverse effect on the existing power grid, both in G2V and V2G operations, especially in coincidence with the daily distribution system peak load. One of the first indicators of the impact of the EVs on the grid is the voltage level along the distribution feeder. Fig. 13 shows the resulting voltage profile: as expected, the voltages are higher during V2G operation and lower in G2V, while in stand-by mode (used as a benchmark) the impact of the load on the medium voltage feeder is negligible. Some interesting observations can be made. From Table 3, it is clearly visible that the impact of the load on the voltage profile of both MV lines

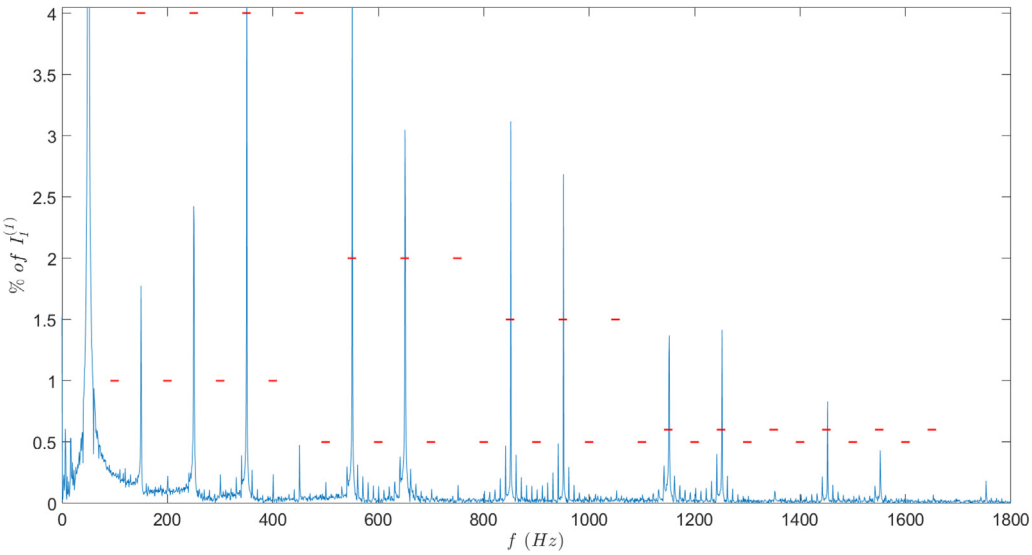

Fig. 12. Twenty stand-by wallboxes harmonics profile. $I_1^{(1)}$ indicates the rms value of the fundamental component of the current related to the phase #1.

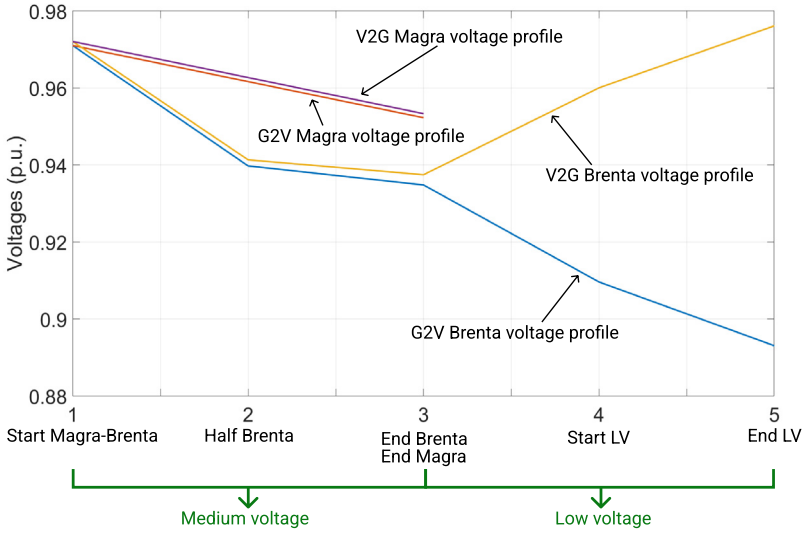

Fig. 13. Twenty charge wallboxes voltage profile.

Table 3
Voltage levels.

Measurement points	Voltage level (p.u.)		
	G2V	*V2G*	*Stand-By*
Start Magra-Brenta - 1	0.97	0.97	0.97
End Magra - 3	0.95	0.95	0.95
Half Brenta - 2	0.94	0.94	0.94
End Brenta - 3	0.93	0.94	0.94
Start LV - 4	0.91	0.96	0.94
End LV - 5	0.89	0.98	0.94

is negligible during the three operational cases. In fact, when all the twenty WBs are in charging mode, the terminal node of the MV feeder results to have a voltage value differing about 1% with respect to the other use cases. Secondly, the 10% of maximum tolerance on the voltage level is not respected at the terminal node of the LV line during the charging procedure: in fact, the voltage is lower than 206 V rms, and this can cause some issues in case other loads are connected at the same node. Moreover, such a low voltage value caused in some occasions the stop of the charging operations by the WB, despite the fact that the minimum voltage required for by the WB to properly work is lower. Furthermore, the control of the internal converter of the charging station works as a constant power load: hence, if the voltages tend to decrease, the currents absorbed will increase, leading to higher power losses on the LV lines. A comparison with a steady state theoretical approach for voltage drop calculation has been done to evaluate the voltage values on the LV grid. The theoretical approximated voltage drop has been calculated as:

$$\Delta V = \sqrt{3} I (R cos\phi + X sin\phi) \quad (1)$$

where:

- ΔV is the voltage drop;
- I is the line current;
- R is the line resistance;
- X is the line reactance;
- ϕ is the line current phase angle.

The value of current used is the fundamental harmonic of the phase current. The voltage at the end of the line, calculated with this approach, is equal to 206.61 V. The value simulated in

Table 4
Power Factor in G2V, V2G and stand-by mode in different system points.

Measurement points	Power factor		
	G2V	*V2G*	*Stand-By*
End Brenta - 3	0.930	0.953	0.362
Start LV - 4	0.954	0.938	0.417
End LV - 5	0.956	0.935	0.417

real-time with PHIL is equal to 0.89 p.u. which is equivalent to 205.54 V; such a non negligible difference could be explained by the presence of current harmonics, that are not considered in the analytical calculation.

4.4. Power factor

As reported in [34], the charging stations should provide a power factor higher than 0.9 when the output of the converters is higher than 50% of the rated output power. In order to know if this requirement is met, the power factor of the WBs has been evaluated in G2V and V2G operations, in different points of the simulated LV grid, to understand the impact of the line parameters on the power factor of the converters when they absorb or inject their maximum power. The calculation of the power factor requires the knowledge of active and apparent power, computed as follows. First of all, the instantaneous power p_{ist} is calculated as shown in Eq. (2):

$$p_{ist} = v_1 \cdot i_1 + v_2 \cdot i_2 + v_3 \cdot i_3 \tag{2}$$

where v_j and i_j are the instantaneous values of the phase-to-neutral voltages and phase currents. Starting from Eq. (2), the active power P is calculated as the average value of p_{ist} considering the period of the fundamental T, as reported in Eq. (3):

$$P = \frac{1}{T}\int_0^T p_{ist}\, dt \tag{3}$$

Then, thanks to the rms value of the phase-to-neutral voltages V_j and the phase currents I_j, retrieved through the measurements, it is possible to evaluate the apparent power S as in Eq. (4):

$$S = (V_1 \cdot I_1) + (V_2 \cdot I_2) + (V_3 \cdot I_3) \tag{4}$$

Finally, the power factor $cos\phi$ that includes the contribution of the harmonics can be calculated as in Eq. (5):

$$cos\phi = P/S \tag{5}$$

The results are then reported in Table 4.

From the EVCS datasheet the nominal power factor is controlled to be almost equal to 1, and after several tests, it resulted being equal to 0.994. The power factor is lower than the nominal value of a single charger. Hence, we can conclude that the lower value is due to both the inductive components introduced by the LV lines and the disturbances on the grid.

Table 4 shows the stand-by power factor as well: this highlights that the total power withdrawn in stand-by could be not negligible in case of real applications with a large number of EVCSs connected, and such a low value of the power factor could lead the EVCS operator to pay economic penalties.

4.5. Power losses

In case of provision of grid services, the amount of energy injected/absorbed by the EVCS is measured at the MV side of the MV/LV distribution transformer, namely the MV Point of Common Coupling (PCC). Hence, the power losses referring to the MV/LV transformer and the LV lines have to be evaluated because they remain a matter of the EVCS operator and may affect both the profitability and the design of the components (such as cables and transformer) of the EVCS . To take in account the power losses caused by the frequency components higher than the fundamental, the waveforms of voltages and currents at different measurement points are collected for calculating the instantaneous power and then the active power as detailed in Eq. (2) and in Eq. (3).

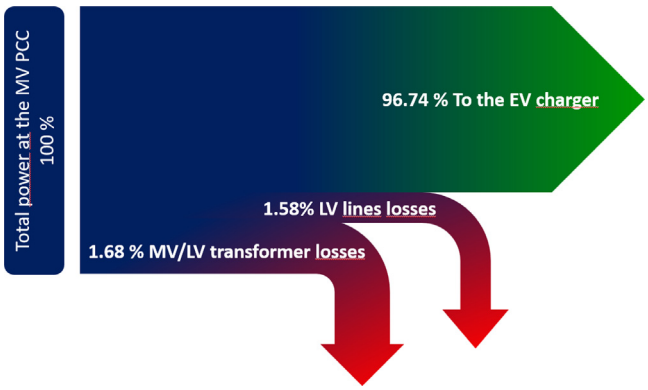

Fig. 14. Sankey diagram of power flows in G2V with losses.

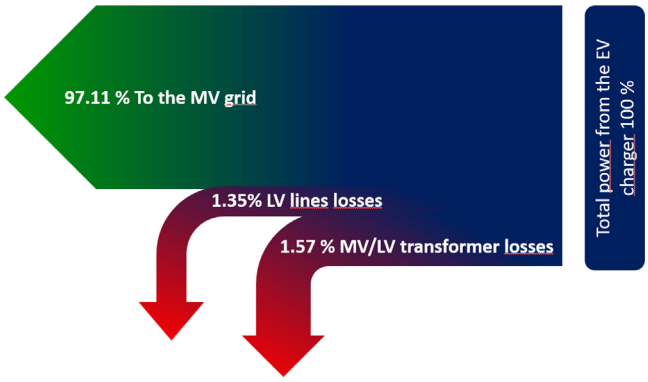

Fig. 15. Sankey diagram of power flows in V2G with losses.

Hence, through power balances, it is possible to evaluate the losses associated to the different components. The power flows and losses can then be effectively visualized through Sankey diagrams. In particular, the power losses of the components of the LV grid portion are depicted in Figs. 14 and 15. As expected, in G2V operation the power losses are slightly higher than in V2G operations.

The measured losses should then be summed to the conversion losses up: the requested power at the connection point will be lower than the power sent by the converters, so it is important to assess the total losses.

Conclusion

This paper presented a study about the impact of EVCS on the upstream MV and LV grid portions. Several indicators have been evaluated by using a layout based on the RTS and PHIL configurations. Regarding the voltage profile, large voltage deviations from the nominal value have been observed, due to the high power withdrawn or injected in the LV grid. In particular, during the G2V operation, the LV side experienced a voltage value below the minimum allowed values.

Due to the high power withdrawn, also the power losses related to the MV/LV transformer and the LV lines were not negligible, reaching 3.2% of the total load in G2V operations and 2.9% of the total power injected in V2G. These values, have to be summed to the conversion losses of the WBs, which can vary depending on the environment temperature and on the power withdrawn. For 10 kW and between −20° and 40°, in V2G the power losses varied respectively from 2.5% to 2.8%, and in G2V from 7.8% to 7.57%.

It is worth noting that both the voltage profile and the losses have been evaluated by taking into account the harmonic contribution of the distorted current injected into the grid by the WBs and this was possible thanks to the presented PHIL layout. In fact, this was made by directly measuring the electrical quantities in the simulated environment, without the need to implement harmonic load flow algorithms as required in the steady state case.

The implemented tests showed the impact of the injected disturbances, highlighting some critical aspects, as well as some operation conditions, such as the emulation of the network resonances in PHIL, which is not revealed by using only standard simulations. In fact, it can be observed a large impact on the harmonic spectrum caused by a 23rd order component due to the interaction among converters, leading to wrong operations in both G2V and V2G working modes.

The same configuration enabled the evaluation of the power factor: in fact, even though the power factor of the single unit is controlled to be almost equal to one, the value of the aggregation of more units needs to be measured. At full load, both for G2V and V2G, the power factor was higher than the limit (0.9), but lower than 1 due to the impact of the LV line parameters and the disturbances injected from the converters. Moreover, the value in stand by was really low for the total load and, considering a higher number of chargers, this value could represent an issue, because the total stand-by power withdrawn is not negligible, and some penalties could be applied.

In this context some general considerations can be drawn: (i) to enhance the efficiency of the LV grid portion, it is worth considering to oversize the MV/LV transformer and the LV lines; (ii) from the harmonic point of view, it seems that the converters tend to be synchronized by the common voltages in input, injecting disturbances with the same phases and leading to the sum of the harmonic components. This phenomena could cause some issues in controlling some harmonic orders, interrupting the charging and discharging operations due to the disturbed waveforms generated. A possible solution to this problem is to connect a filter before sending the input voltages, which correspond to decouple the converters from the network.

The presented approach has been used as a first step to understand how multiple WBs connected close to each other in a parking lot will impact the future networks. A possible limitation of the study is represented by the ideal sum of the chargers contribution inside the simulation. Moreover, the tests have been done in the worst case scenario, with the chargers working close to their maximum power, to assess the maximum impact on the grid. For these reasons, in order to further verify the hypothesis, especially for the harmonics summation, future work will assess the interaction between two or more units of the same EVCS, testing both the converters with different combinations of power set-points to check if the power level has an impact on the harmonics magnitude, sum or cancellation.

CRediT authorship contribution statement

Giorgio Benedetto: Methodology, Software, Formal analysis, Investigation, Data curation, Writing – original draft, Writing – review & editing, Visualization. **Ettore Bompard:** Resources, Writing – review & editing, Supervision, Funding acquisition. **Andrea Mazza:** Conceptualization, Methodology, Formal analysis, Writing – original draft, Writing – review & editing, Visualization. **Enrico Pons:** Conceptualization, Methodology, Software, Investigation, Writing – original draft, Writing – review & editing. **Rémi Jaboeuf:** Validation. **Paolo Tosco:** Conceptualization, Validation, Resources, Supervision, Funding acquisition. **Marco Zampolli:** Validation, Investigation.

Declaration of competing interest

The authors declare that they have no known competing financial interests or personal relationships that could have appeared to influence the work reported in this paper.

Data availability

The data used for this work are confidential.

References

[1] G. Chicco, A. Ciocia, P. Colella, P. Di Leo, A. Mazza, S. Musumeci, E. Pons, A. Russo, F. Spertino, Introduction—Advances and Challenges in Active Distribution Systems, Springer International Publishing, Cham, 2022, pp. 1–42,
[2] Deloitte, Deloitte insights, 2020.
[3] E. Outlook, IEA, Paris, 2020, URL https://www.iea.org/reports/global-ev-outlook-202.
[4] E. Commission, D.-G. for Energy, Effect of Electromobility on the Power System and the Integration of RES : Study S13, Publications Office, 2019.
[5] O.C. Onar, A. Khaligh, Grid interactions and stability analysis of distribution power network with high penetration of plug-in hybrid electric vehicles, in: 2010 Twenty-Fifth Annual IEEE Applied Power Electronics Conference and Exposition (APEC), 2010, pp. 1755–1762.
[6] A. Annamraju, S. Nandiraju, Coordinated control of conventional power sources and PHEVs using jaya algorithm optimized PID controller for frequency control of a renewable penetrated power system, Prot. Control Mod. Power Syst. 4 (1) (2019) 1–13.
[7] A.W. Thompson, Y. Perez, Vehicle-to-Everything (V2X) energy services, value streams, and regulatory policy implications, Energy Policy 137 (2020) 111136, http://dx.doi.org/10.1016/j.enpol.2019.111136.
[8] N.B. Arias, S. Hashemi, P.B. Andersen, C. Træholt, R. Romero, Assessment of economic benefits for EV owners participating in the primary frequency regulation markets, Int. J. Electr. Power Energy Syst. 120 (2020) 105985.
[9] A. Kieldsen, S. Martinenas, T.M. Sørensen, Efficiency test method for electric vehicle chargers.
[10] M.N. Iqbal, L. Kütt, K. Daniel, B. Asad, P. Shams Ghahfarokhi, Estimation of harmonic emission of electric vehicles and their impact on low voltage residential network, Sustainability 13 (15) (2021) 8551, http://dx.doi.org/10.3390/su13158551, URL https://www.mdpi.com/2071-1050/13/15/8551, Number: 15 Publisher: Multidisciplinary Digital Publishing Institute.
[11] T. Slangen, T. van Wijk, V. Ćuk, S. Cobben, The propagation and interaction of supraharmonics from electric vehicle chargers in a low-voltage grid, Energies 13 (15) (2020) 3865, http://dx.doi.org/10.3390/en13153865, URL https://www.mdpi.com/1996-1073/13/15/3865, Number: 15 Publisher: Multidisciplinary Digital Publishing Institute.
[12] I. Jayawardana, C.N.M. Ho, Y. Zhang, A comprehensive study and validation of a power-HIL testbed for evaluating grid-connected EV chargers, IEEE J. Emerg. Sel. Top. Power Electr. 10 (2) (2022) 2395–2410, http://dx.doi.org/10.1109/JESTPE.2021.3093303, Conference Name: IEEE Journal of Emerging and Selected Topics in Power Electronics.
[13] R. Mahmud, M. Jun, X. Zhu, P. Mishra, A.A.S. Mohamed, A. Meintz, Grid impact analysis using controller-hardware-in-the-loop for high-power vehicle charging stations, Sustain. Energy, Grids Netw. 32 (2022) 100883, http://dx.doi.org/10.1016/j.segan.2022.100883.
[14] Global Real-Time Simulation Lab @ PoliTo – An internationally interconnected real-time simulationlab, URL http://g-rtslab.polito.it/.
[15] T.S. Ustun, J. Hashimoto, K. Otani, Impact of smart inverters on feeder hosting capacity of distribution networks, IEEE Access 7 (2019) 163526–163536, http://dx.doi.org/10.1109/ACCESS.2019.2952569.
[16] D.C. Silva, B.F. Musse, N.L. Silva, P.M. de Almeida, J.G. de Oliveira, Hardware in the loop simulation of shunt active power filter (SAPF) utilizing RTDS and dSPACE, in: 2017 Brazilian Power Electronics Conference (COBEP), 2017, pp. 1–6, http://dx.doi.org/10.1109/COBEP.2017.8257402.
[17] L. Ibarra, A. Rosales, P. Ponce, A. Molina, R. Ayyanar, Overview of real-time simulation as a supporting effort to smart-grid attainment, Energies 10 (6) (2017).

[18] C. Edrington, M. Steurer, J. Langston, T. El-mezyani, K. Schoder, Role of power hardware in the loop in modeling and simulation for experimentation in power and energy systems, Proc. IEEE 103 (2015) 1–9.
[19] Z. Taylor, H. Akhavan-Hejazi, H. Mohsenian-Rad, Power hardware-in-loop simulation of grid-connected battery systems with reactive power control capability, 2017, pp. 1–6.
[20] N. Ninad, E. Apablaza-Arancibia, M. Bui, J. Johnson, Commercial PV inverter IEEE 1547.1 ride-through assessments using an automated PHIL test platform, Energies 14 (21) (2021).
[21] F. Huerta, R. Tello, M. Prodanovic, Real-time power-hardware-in-the-loop implementation of variable-speed wind turbines, IEEE Trans. Ind. Electron. PP (2016) 1.
[22] J.-H. Jung, Real-time and power hardware-in-the-loop simulation of PEM fuel cell stack system, J. Power Electron. 11 (2011).
[23] I. Jayawardana, C. Ho, Y. Zhang, A comprehensive study and validation of a power-HIL testbed for evaluating grid-connected EV chargers, IEEE J. Emerg. Sel. Top. Power Electr. PP (2021) 1.
[24] L. De Herdt, A. Shekhar, Y. Yu, G. Chandra Mouli, J. Dong, P. Bauer, Power hardware-in-the-loop demonstrator for electric vehicle charging in distribution grids, in: 2021 IEEE Transportation Electrification Conference & Expo (ITEC), IEEE, United States, 2021, pp. 679–683.
[25] M. Pokharel, C.N.M. Ho, Stability analysis of power hardware-in-the-loop architecture with solar inverter, IEEE Trans. Ind. Electron. 68 (5) (2020) 4309–4319.
[26] A. Riccobono, A. Helmedag, A. Berthold, N.R. Averous, R.W. De Doncker, A. Monti, Stability and accuracy considerations of power hardware- in-the-loop test benches for wind turbines, IFAC-PapersOnLine 50 (1) (2017) 10977–10984, 20th IFAC World Congress.
[27] A. Mazza, E. Pons, E. Bompard, G. Benedetto, P. Tosco, M. Zampolli, R. Jaboeuf, A power hardware-in-the-loop laboratory setup to study the operation of bidirectional electric vehicles charging stations, in: 2022 International Conference on Smart Energy Systems and Technologies (SEST), 2022, pp. 1–6, http://dx.doi.org/10.1109/SEST53650.2022.9898502.
[28] E. Guillo-Sansano, M.H. Syed, A.J. Roscoe, G.M. Burt, F. Coffele, Characterization of time delay in power hardware in the loop setups, IEEE Trans. Ind. Electron. 68 (3) (2020) 2703–2713.
[29] Cinergia, EL15. External Operation. Inputs and Outputs, v8.3 ed., 2018.
[30] P. Staats, W. Grady, A. Arapostathis, R. Thallam, A statistical method for predicting the net harmonic currents generated by a concentration of electric vehicle battery chargers, IEEE Trans. Power Deliv. 12 (3) (1997) 1258–1266.
[31] A. Lucas, Fast charging diversity impact on total harmonic distortion due to phase cancellation effect, 2017.
[32] P. Staats, W. Grady, A. Arapostathis, R. Thallam, A statistical analysis of the effect of electric vehicle battery charging on distribution system harmonic voltages, IEEE Trans. Power Deliv. 13 (2) (1998) 640–646.
[33] C. Stackler, N. Evans, L. Bourserie, F. Wallart, F. Morel, P. Ladoux, 25 KV–50 Hz railway power supply system emulation for power-hardware-in-the-loop testings, IET Electr. Syst. Transp. 9 (2) (2019) 86–92, http://dx.doi.org/10.1049/iet-est.2018.5011.
[34] Technical requirements for connecting small scale PV (ssPV) systems to low voltage distribution networks, 2014.
[35] IEEE, IEEE standard conformance test procedures for equipment interconnecting distributed energy resources with electric power systems and associated interfaces, in: IEEE Std 1547.1-2020, IEEE, 2020.